This is the Pre-Published Version.

This version of the article has been accepted for publication, after peer review (when applicable) and is subject to Springer Nature's AM terms of use (https://www.springernature.com/gp/open-research/policies/accepted-manuscript-terms), but is not the Version of Record and does not reflect post-acceptance improvements, or any corrections. The Version of Record is available online at: http://dx.doi.org/10.1007/s10570-020-03408-y.

A Theoretical Model to Investigate the Performance of Cellulose Yarns Constrained to Lie on a Moving Solid Cylinder

Rong Yin[a,b*], Xiaoming Tao[b], Warren Jasper[a]

[a] *Wilson College of Textiles, North Carolina State University, Raleigh, NC 27606, USA*

[b] *Institute of Textiles and Clothing, The Hong Kong Polytechnic University, Hong Kong, 999077, China*

*Correspondence E-mail: ryin@ncsu.edu (R. Yin)

Abstract:

Cellulose fibers, such as cotton and linen, are abundant in farmer's fields. The traditional bottom-up technology to process these short staple fibers is spinning. State-of-the-art spinning technology requires not only high throughput processing of the cellulose fibers, but also the addition of functionalities and value into the supply chain. Recently, a modified ring spinning system has been developed which introduces a false twist into a traditional ring spinning frame. The modified system produces cellulose yarns that have a high strength but low twist, and a soft hand similar to cashmere. Unlike traditional textile finishing treatments which consume plenty of chemicals, water, and energy, this method is purely physical and sustainable. The superior properties of the modified cellulose yarns are attributed to the modified yarn morphology and structure. Theoretical investigation is, therefore, important in understanding of the spinning mechanisms of the modified ring spinning process that changes the morphology and structure of the cellulose yarns. In this paper, yarn behavior constrained to lie on a moving solid cylinder was theoretically and experimentally investigated. Equations of motion were derived based on the Cosserat theory and numerical solutions in steady-state were obtained in terms of yarn spatial path, yarn tension, twist distribution, yarn bending, and torsional moments. Effects of various spinning parameters including wrap angle, speed of the moving cylinder, yarn diameter, yarn tension, yarn twist, and frictional coefficient, on yarn behavior were discussed. The results suggested that in most cases the bending and torsional moments are of the same order of magnitude, and thus the effect of bending cannot be neglected. Experiments in the modified ring spinning system were conducted to verify the theoretical work, and good agreement has been made. Some simulation results of this study were compared with the results of earlier models as well as with experimental data, and it was found that the current model can obtain a more accurate prediction than previous models in terms of yarn twist and tension. The results gained from this study will enrich our understanding of the spinning mechanism of the modified ring spinning process and better handle of cellulose fibers for functional and value-added applications.

Keywords: cellulose fiber, yarn tension, yarn twist, mathematical modeling, modified ring spinning

1. Introduction

Cellulose fibers are abundant in farmer's fields, with two of the most common examples being cotton and linen (César et al. 2015; Liu et al. 2019; Morán et al. 2008). The traditional bottom-up technology of natural cellulose fibers is spinning. Spinning (Hearle et al. 1969) is a fundamental method for manufacturing long strands of staple yarn from cellulose fibers of cotton, rayon, and linen. Among all of the spinning technologies, ring spinning (Lawrence 2010) continues to predominate in the yarn manufacturing industry due to its high yarn quality and flexibility in materials and yarn counts. During the yarn manufacturing process, twisting increases fiber coherence and imparts strength to a staple yarn. The degree of twist in the final yarn is important not only because of its influence on yarn characteristics such as strength, hand, and hairiness, but also because it determines the yarn's structure by manipulating a bundle of separated short fibers and assembling them into a consolidated yarn. Yarn tension also plays an important role in yarn formation and resultant yarn quality (Yin and Gu 2011a). Although yarn tension cannot exceed the strength of the yarn at any instant the tension at which the yarn is formed affects its structure and properties. At a macro level, power consumption in the spinning process is proportional to the yarn tension, it is, therefore, important to balance the tension level to minimize the power consumption while maximizing the yarn quality (Fraser 1993).

Much valuable work has been carried out to theoretically study the spinning process in ring (Stump and Fraser 1996; Tang et al. 2011), rotor (Guo et al. 2000; Xu and Tao 2003), air jet (Grosberg et al. 1987), etc. For instance, Fraser established the mathematical model and boundary conditions of ballooning yarn, and discussed the relationship between the traveler mass and yarn tension in detail (Fraser 1993). Xu and Tao proposed a theoretical model to study yarn tension and twist distributions in rotor spinning (Xu and Tao 2003). Miao and Chen proposed a method of which the governing equation of twist distribution of a straight yarn is a wave equation (Miao and Chen 1993). van der Heijden and Thompson investigated the bifurcations or instabilities of twisted yarn, as twisted elastic rods, under specific conditions (van der Heijden and Thompson 2000).

State-of-the-art spinning technology requires not only high throughput processing of the cellulose fibers, but also the addition of functionalities and value into the supply chain. Continuous improvements have been made in the ring spinning sector due to the requirement of novel features or improving yarn quality. In particular, a modified ring spinning system has been proposed (Tao and Yin 2019) and studied (Guo et al. 2015; Hua et al. 2013; Yang et al. 2007; Yin et al. 2020a; Yin et al. 2020b) to produce a high strength but low twist and soft hand cellulose yarns. The hand of cellulose fabrics made by the modified spinning method is similar to cashmere, which greatly improves the added value of the cellulose fibers. Unlike traditional textile finishing treatments (César et al. 2015; Kim and Son 2005; Liu et al. 2018) in which consume plenty of chemicals, water, and energy, this method is purely physical and sustainable. The key is to attach an additional device which is furnished with an additional false twisting unit. Theoretical investigations are, therefore, important in understanding of the spinning mechanisms of the modified ring spinning process which changes the morphology and structure of the cellulose yarns. Feng et al. proposed a mechanical model to study flexible yarn performance on a moving solid cylinder and treated the model as an initial value problem (Feng et al. 2012). Yin et al. further investigated yarn performance in the proposed modified system by means of twist generation and twist propagation (Yin et al. 2016).

However, in those works, the bending moment was omitted for simplification purposes. In many cases, the bending and torsional moments are of the same order of magnitude, and ignoring bending may lead to errors in the derived results and deviation in model prediction from experiment. Therefore, the investigations associated with yarn bending are conducted in this work. Equations of yarn motion are established based on Cosserat theory (van der Heijden et al. 2002) and the boundary value problems are numerically solved by the Newton-Raphson method. Then, the effects of various spinning parameters in terms of wrap angle speed of the moving cylinder, yarn diameter, yarn tension, yarn twist, and frictional coefficient, on yarn tension and twist distributions, yarn spatial position, bending and torsional moments lying on a cylinder are discussed. Next, experiments in the modified ring spinning system are described, and the experimental results are discussed. In addition, some simulation results of this study are compared with the results of earlier models and experimental data. The results gained from this study will enrich our understanding of the spinning mechanism of a modified ring spinning process and improve the hand of cellulose fabrics

2. Theoretical

A modified ring spinning system has been proposed by introducing a moving solid cylinder into the conventional ring spinning frame, shown in Fig. 1, which acts as a false twister and adds a false twist into the yarn. The existence of a false twist changes yarn tension and twist distributions in the spinning process. Additional false twist is introduced into the yarn above the false twister due to the interaction between the yarn and moving solid cylinder, while the presence of false twist is totally negated below the false twister.

The whole system can be divided into 5 zones. The first zone is from the front rollers A to the entrance point B of the solid cylinder. The yarn path in this zone can be deemed as a straight line. Next, the yarn slides over the convex surface of the solid cylinder. Both yarn tension and twist distributions are varied evidently. The next zone contains the yarn path from the exit point C of the solid cylinder to the yarn guide D. The yarn path in this zone can also be deemed as a straight line. The following zone includes the yarn path from the yarn guide D to the traveler. The ballooning effect in this zone has been widely reported in the literature (Fraser 1993; Yin and Gu 2011a; Yin and Gu 2011b; Yin et al. 2010). The last zone is from the traveler to the winding point on the bobbin, which can be treated as a straight line as well. In this work, we mainly focus on the behavior of the twisting yarn constrained to the moving solid cylinder, which is the second zone of the whole system.

The equilibrium configurations describing the steady-state motion of a twisting yarn were derived under several simplifying assumptions. 1) The yarn is assumed to be inextensible since twisting of yarn is the dominating phenomenon, while the deformation in the yarn's axial direction is small can be ignored; 2) A uniform yarn is assumed with a single linear density and cross-sectional area; 3) The weight of yarn is relatively small when compared with other forces can be neglected; 4) The moving cylinder has a much greater rigidity than the yarn can be regarded as non-deformable; 5) The moving cylinder is smooth with a constant radius of curvature; 6) A linear relationship between the yarn twist and torque is assumed based on solid mechanics as well as previous experimental results (Bennett and Postle 1979); 7) The model was built in a steady-state, thus time-dependent terms in the equations are ignored; 8) The study deals with stable twisting processes where no mechanical instability or bifurcation occurs. Validation and justification of these assumptions can be found in Supplementary Information.

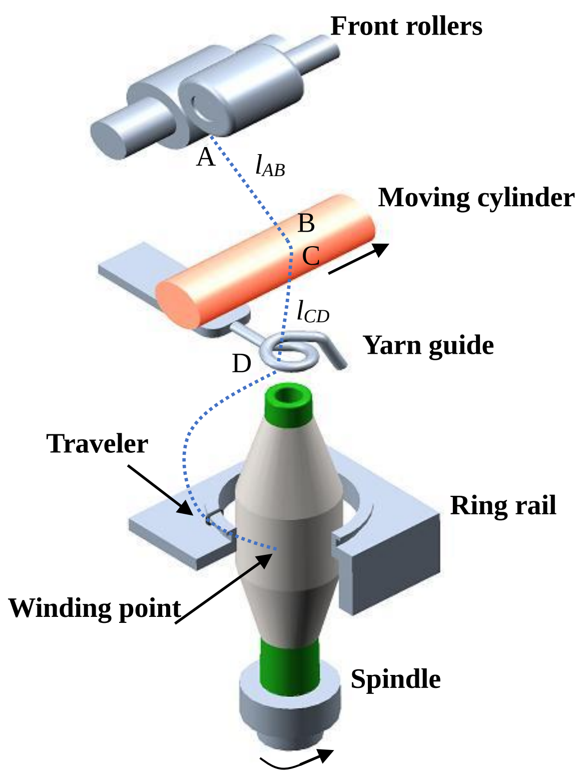

Fig. 1 A modified ring spinning system

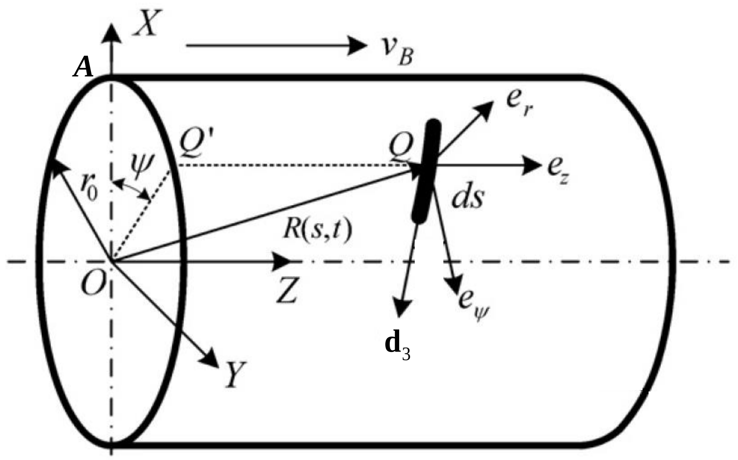

Fig. 2 A yarn segment in the coordinate system

2.1 Mathematical modeling

Consider an arbitrary point **Q** of the yarn, which is at a distance *s* measured along the yarn from the initial contacting point **A (*s=0*)**, as shown in Fig. 2. For the convenience of analysis, a fixed cylindrical coordinate system is selected with base vectors $\{\mathbf{e_r}, \mathbf{e_\psi}, \mathbf{e_z}\}$. The origin of coordinate **O** coincides with the center of the initial contact surface, and the z axis of the system is in line with the central axis of the rigid cylinder with its positive direction towards the moving direction (v_b in Fig. 2). Let r_0, ψ, z be the cylindrical coordinates corresponding to the coordinate frame and $\mathbf{R}(s) = r_0\mathbf{e}_r + z\mathbf{e}_z$ be the position vector of Q relative to the origin O.

Because of inextensibility $\dot{\mathbf{R}}(s) = d\mathbf{R}/ds$ is the unit tangent to the centerline at *s*, which is denoted by $\mathbf{d}_3(s)$. As shown in Fig. 3, a right-handed orthonormal basis $\{\mathbf{d}_1, \mathbf{d}_2, \mathbf{d}_3\}$ of so-called directors is defined by taking $\mathbf{d}_2 = \mathbf{d}_3 \times \mathbf{d}_1$. The configuration of the yarn is fully determined if the vectors $\mathbf{d}_i$, *i=1, 2, 3* are specified, and vice versa. The vector $\mathbf{R}(s)$ can be derived by solving the differential equation

$$\dot{\mathbf{R}}(s) = \mathbf{d}_3(s), \quad \mathbf{R}(0) = 0 \tag{1}$$

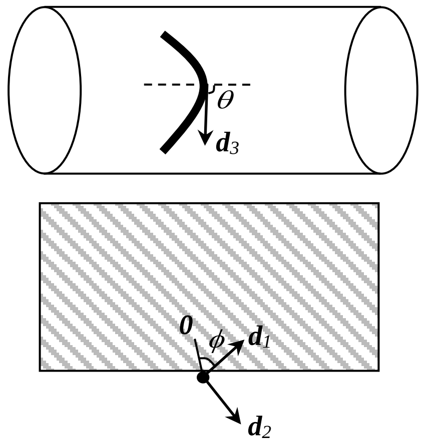

Fig. 3 The angles used to describe a twisted yarn segment

This moving coordinate system is related to a fixed cylindrical system $\{\mathbf{e_r}, \mathbf{e_\psi}, \mathbf{e_z}\}$ using the following notation: $\mathbf{d}_i = d_{ir}\mathbf{e}_r + d_{i\psi}\mathbf{e}_\psi + d_{iz}\mathbf{e}_z$. Due to the constraint of the yarn position, there are two degrees of freedom for the director frame $\{\mathbf{d}_i\}$. Therefore, two angles, θ and ϕ are introduced as follows,

$$\begin{aligned}
\mathbf{d}_1 &= \sin\phi\mathbf{e}_r - \cos\phi\cos\theta\mathbf{e}_\psi + \cos\phi\sin\theta\mathbf{e}_z \\
\mathbf{d}_2 &= \cos\phi\mathbf{e}_r + \sin\phi\cos\theta\mathbf{e}_\psi - \sin\phi\sin\theta\mathbf{e}_z \\
\mathbf{d}_3 &= \sin\theta\mathbf{e}_\psi + \cos\theta\mathbf{e}_z
\end{aligned} \tag{2}$$

where $\mathbf{d}_1$ is a radial line, perpendicular to the strand axis joined to any straight line parallel to the axis marked on the surface of the initially straight untwisted strand, θ is the deviation angle formed between the unit vectors $\mathbf{d}_3$ and $\mathbf{e}_z$, and ϕ is the internal twist angle of $\mathbf{d}_1$ about $\mathbf{d}_3$.

Since $\mathbf{d}_1$, $\mathbf{d}_2$, and $\mathbf{d}_3$ are orthonormal, there exists a vector function $\mathbf{u}(s)$, the deformation, such that

$$\dot{\mathbf{d}}_i = \mathbf{u} \times \mathbf{d}_i \quad i = 1,2,3 \tag{3}$$

The components of $\mathbf{u}(s)$ with respect to $\{\mathbf{d}_i\}$ are the strains of our theory whose components are the curvatures and the twist. They are denoted by

$$\mathbf{u} = u_1\mathbf{d}_1 + u_2\mathbf{d}_2 + u_3\mathbf{d}_3 \tag{4}$$

where u_1 and u_2 are curvatures of the projections of the strained centerline on the planes $(\mathbf{d}_2, \mathbf{d}_3)$ and $(\mathbf{d}_1, \mathbf{d}_3)$, respectively. The strain u_3 is the twist and measures the rate of rotation about the body axis of the yarn.

The following equation is readily derived from the director frame equation expressed in cylindrical coordinates by using the equations for d_{1r}

$$u_3 = \dot{\phi} + \dot{\psi}\cos\theta \tag{5}$$

where $\dot{\phi} = 2\pi T$, T is the inserted number of twists per unit length of yarn.
Eq. (5) expresses the usual partition of twist, u_3, into internal twist and space curve torsion. $\dot{\phi}$ means the initial torsion in the straight strand before its axis is deformed into a curved path. $\dot{\psi}\cos\theta$ is the torsion due to the rotation of the principal plane of curvature (Love 1927).

Suppose $\mathbf{d}_1$ is equal to the principal normal and hence, $\mathbf{d}_2$ to the binormal of $\mathbf{R}(s)$, τ is the torsion of the centerline of the yarn and the deformation vector, now also called the Darboux vector, becomes $\mathbf{u} = (0, \kappa, \tau)$. The corresponding equations then are the Frenet–Serret equations of differential geometry:

$$\begin{aligned} \dot{\mathbf{n}} &= \tau\mathbf{b} - \kappa\mathbf{t} \\ \dot{\mathbf{b}} &= -\tau\mathbf{n} \\ \dot{\mathbf{t}} &= \kappa\mathbf{n} \end{aligned} \tag{5}$$

where $\mathbf{n} = \ddot{\mathbf{R}}/|\ddot{\mathbf{R}}|$, $\mathbf{b} = \dot{\mathbf{R}} \times \ddot{\mathbf{R}}/|\dot{\mathbf{R}} \times \ddot{\mathbf{R}}|$ and $\mathbf{t} = \dot{\mathbf{R}}$ be the normal, binormal and tangent base vector of the yarn centerline, respectively.

Let the internal forces and moments along the rod be $\mathbf{p}$ and $\mathbf{m}$, respectively, such that the equilibrium equations of the yarn are given by

$$\begin{aligned} &\dot{\mathbf{p}} + \mathbf{f} = 0 \quad \text{(force balance)} \\ &\dot{\mathbf{m}} + \dot{\mathbf{R}} \times \mathbf{p} + \mathbf{m}_{\mathbf{f}} = 0 \quad \text{(moment balance)} \end{aligned} \tag{6}$$

where $\mathbf{f}$ and $\mathbf{m_f}$ are external loading and torque acting on the yarn element, respectively.

The internal forces and moments can be expressed in the director frame $\{\mathbf{d}_i\}$ as follows,

$$\mathbf{p} = p_1\mathbf{d}_1 + p_2\mathbf{d}_2 + p_3\mathbf{d}_3$$

$$\mathbf{m} = m_1\mathbf{d}_1 + m_2\mathbf{d}_2 + m_3\mathbf{d}_3 \tag{7}$$

where p_3 be the tension in the yarn, and p_1, p_2 be components of the shear force acting on the cross-section perpendicular to the yarn axis. For a flexible yarn, the bending stiffness is neglected, therefore the shear force of the yarn should be zero as well. In this study, the bending stiffness is now taken into consideration, so the yarn is not perfectly flexible, the shear force of the yarn should not be zero.

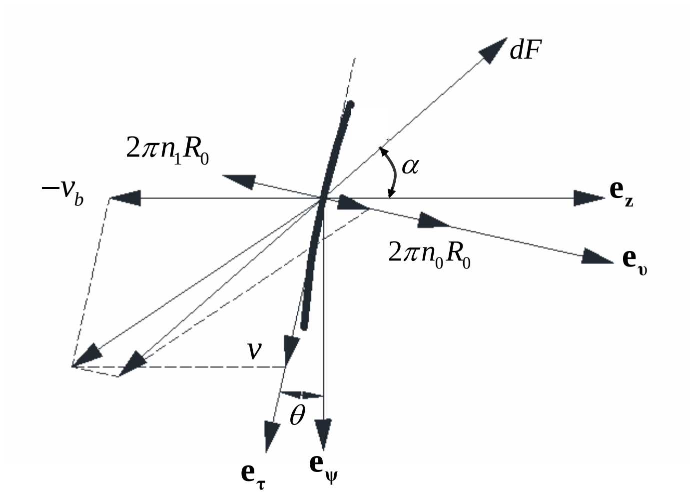

Fig. 4 Analysis on yarn motions

The external forces include normal reaction force and frictional force. Thus, if μ is the coefficient of friction, and N is the magnitude of the normal reaction of the cylinder on the yarn, then

$$\mathbf{f} = \mathbf{N} + \mathbf{F} = N\mathbf{e}_r + \mu N\left(\cos\alpha\mathbf{e}_v - \sin\alpha\mathbf{t}\right) \tag{8}$$

where $\mathbf{e}_v$ is expressed as $\mathbf{e}_v = \mathbf{e}_r \times \mathbf{t}$, $\alpha = arc\tan\dfrac{v_b\cos\theta + v}{v_b\sin\theta + 2\pi R_0(n_1 - n_0)}$ be the friction angle between the direction of friction force and the unit vector $\mathbf{e}_v$, v be the yarn delivery speed, v_B be the moving speed of the cylinder $\mathbf{e}_z$, n_0 be the rotational speed of the yarn generated by the twister, and n_1 be the rotational speed of the yarn generated by the moving cylinder, as shown in Fig. 4.

The frictional moment can be expressed as follows,

$$\mathbf{m}_\mathbf{f} = \mu N \cos\alpha R_0 \mathbf{t} \tag{9}$$

where R_0 is the radius of yarn.

The scalar formulas of Eq. (6) can be written after some rearrangement as follows,

$$\begin{cases} (\dot{p}_1 - p_2\tau + p_3\kappa)(\mathbf{n}\cdot\mathbf{e}_\mathbf{v}) + (\dot{p}_2 + p_1\tau)(\mathbf{b}\cdot\mathbf{e}_\mathbf{v}) + \mu N\cos\alpha = 0 \\ (\dot{p}_1 - p_2\tau + p_3\kappa)(\mathbf{n}\cdot\mathbf{e}_\mathbf{r}) + (\dot{p}_2 + p_1\tau)(\mathbf{b}\cdot\mathbf{e}_\mathbf{r}) + N = 0 \\ \dot{p}_3 - p_1\kappa - \mu N\sin\alpha = 0 \\ \tau m_2 - \kappa m_3 + p_2 = 0 \\ \dot{m}_2 + p_1 = 0 \\ \dot{m}_3 + \mu N\cos\alpha R_0 = 0 \end{cases} \tag{10}$$

Linear constitutive relations between the forces and deformations are assumed,

$$u_1 = \frac{1}{B_1}\mathbf{m}\cdot\mathbf{d}_1,\quad u_2 = \frac{1}{B_2}\mathbf{m}\cdot\mathbf{d}_2,\quad u_3 = \frac{1}{K}\mathbf{m}\cdot\mathbf{d}_3 \tag{11}$$

where B_1 and B_2 are the bending stiffnesses about $\mathbf{d}_1$ and $\mathbf{d}_2$, respectively, and K is the torsional stiffness.

This leads to

$$m_2 = B\kappa,\quad m_3 = K\tau \tag{12}$$

The assumptions for bending and twisting of yarns, the equations for the bending and torsional stiffness, respectively, of a circular shaft are

$$K = \frac{1}{2}\pi G R_0^{\,4},\quad B = \frac{1}{4}\pi E R_0^{\,4} \tag{13}$$

where E is Young's modulus, and G is the shear modulus.

If υ is Poisson's ratio, then $G = E/2(1+\upsilon)$ and with $\upsilon = 0.3$, this leads to

$$B = 1.3K \tag{14}$$

The actual stiffnesses of yarns are smaller than would be computed by Eq. (13). However, the ratio of K to B derived by Eq. (14) is in approximate agreement with the experiment

(Tandon et al. 1995). It should be noted that these stiffness values have the same order of magnitude.

At this point, a model with three unknowns (p_3, θ, T) and three equations relating them have been derived so far, while p_1, p_2, κ and τ are functions of θ and T. In addition, the rotational speed n_1 is an unknown constant value. Therefore, a total of four boundary conditions are necessary to make this problem solvable.

2.2 Boundary conditions

One boundary equation can be derived based on the geometrical condition of the modified spinning system, as shown in Fig. 5. The line AD formed by the delivery rollers at point A and the yarn guide at point D are perpendicular to the centerline of the moving solid cylinder (line GH). Since the length of line AB formed by the delivery rollers at point A and the entrance point B and line CD formed by the exit point C and the yarn guide at point D are at least one order of magnitude higher than that of curve BC, $l_{AB} \approx l_{AK}$ and $l_{CD} \approx l_{DK}$. Approximately, the deviation angles for line AB and CD follow,

$$\frac{\sin\theta_{AB}}{\sin\theta_{CD}} = -\frac{l_{CD}}{l_{AB}} \tag{15}$$

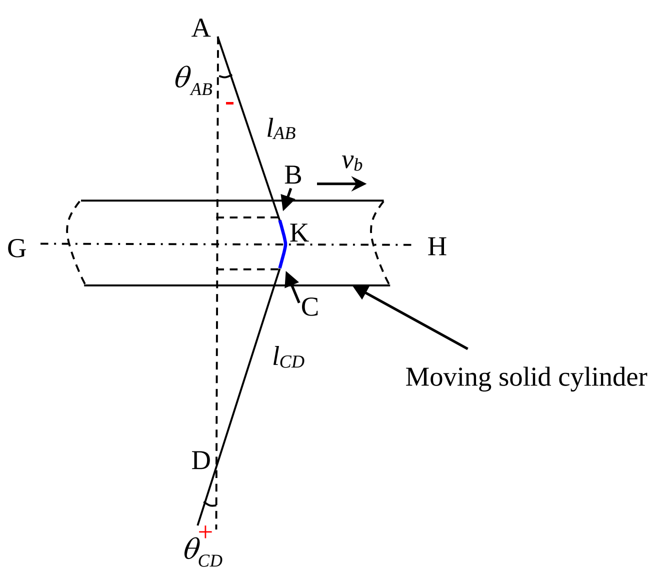

Fig. 5 Geometrical boundary conditions

Another boundary equation is directly obtained from the kinematic formula (Yin et al. 2018) as follows

$$n_1 = (T_{AB} - kT_{CD})\eta v \tag{16}$$

where k and η are propagation coefficients of twist trapping and congestion, respectively. Details of the derivation can be found in Supplementary Information.

The other two boundary values are the tension and twist at either line AB or line CD, i.e. $p_{3\mathrm{AB}}$ and T_{CD}, which can be measured by using high-speed camera and tension meter systems.

2.3 Bending and torsional moments

According to Equation 12, the bending and torsional moments are dependent on 4 factors, namely, *B*, *K*, κ, and τ. And from Equation 14, we know that *B* and *K* are of the same order of magnitude. Therefore, whether the bending moment can be neglected or not is decided by the curvature and torsion of the yarn. The relationship between bending and torsional moments are displayed in Fig. 6. For a twisted yarn lying on a solid cylinder, the curvature of the yarn is largely dependent on the radius of the solid cylinder, while the yarn torsion is associated with the yarn twist inserted. In the case of a high twist yarn lying on a cylinder with a large radius, the yarn curvature is much smaller than the yarn torsion, therefore the yarn bending moment can be neglected. In the case of a low twist yarn lying on a cylinder with a small radius, the yarn bending moment must be taken into account since the yarn bending moment is of the same order of magnitude or larger than the torsional moment. Since the yarn twist changes during interaction with the solid cylinder, it is necessary to investigate the effect of system parameters on the bending and torsional moments as well as the yarn performance. In the following analysis, the governing and boundary equations are normalized to minimize the number of variables.

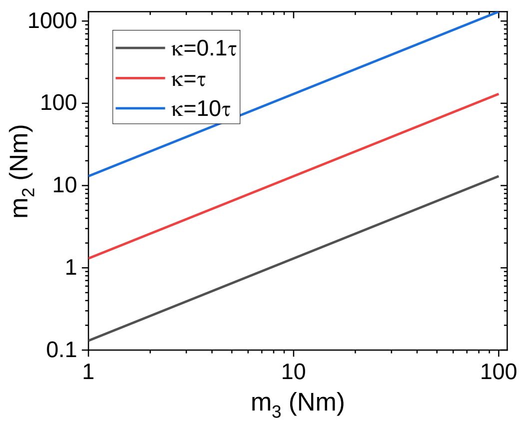

Fig. 6 The relationship between bending and torsional moments

2.4 Dimensionless equations

The normalized variables introduced here are similar to those used by (Fraser and Stump 1998). Lengths are normalized against the cylinder radius r_0, forces are normalized against K/r_0^2, which is a measure of the magnitude of forces required to bend and twist the yarns. Moments are normalized against K/r_0.

$$\begin{aligned}
&\bar{\mathbf{R}} = \frac{\mathbf{R}}{r_0} = \mathbf{e}_r + \frac{z}{r_0}\mathbf{e}_z = \bar{r}_0\mathbf{e}_r + \bar{z}\mathbf{e}_z, \bar{s} = \frac{s}{r_0} \\
&\bar{R}_0 = \frac{R_0}{r_0}, \bar{r}_0 = 1, \bar{l}_{AB} = \frac{l_{AB}}{r_0}, \bar{l}_{CD} = \frac{l_{CD}}{r_0} \\
&\bar{v} = \frac{v r_0^2}{K}, \bar{v}_b = \frac{v_b r_0^2}{K}, \bar{n}_0 = \frac{n_0 r_0^3}{K}, \bar{n}_1 = \frac{n_1 r_0^3}{K} \\
&\bar{T}_{AB} = T_{AB} r_0, \bar{T}_{CD} = T_{CD} r_0, \bar{T} = T r_0 \\
&\overline{p_{3AB}} = \frac{p_{3AB} r_0^2}{K}, \overline{p_{3CD}} = \frac{p_{3CD} r_0^2}{K}, \bar{p} = \frac{p r_0^2}{K}, \bar{N} = \frac{N r_0^3}{K} \\
&\bar{K} = 1, \bar{B} = \frac{B}{K}
\end{aligned} \tag{17}$$

The governing equations in the dimensionless form become

$$-\frac{\sin\theta\theta'}{\bar{\kappa}}(\sin\theta\,\overline{p'}_1 - \overline{p_2}\,\bar{\tau} + \overline{p_3}\,\bar{\kappa}) + \frac{\sin^2\theta}{\bar{\kappa}}(\sin\theta\,\overline{p'}_2 + \overline{p_1}\,\bar{\tau}) + \mu\bar{N}\cos\alpha = 0$$

$$-\bar{\kappa}\,\overline{p_1} + \sin\theta\,\overline{p'}_3 - \mu\bar{N}\sin\alpha = 0 \tag{18}$$

$$\sin\theta\,\bar{\tau}' + \mu\bar{N}\cos\alpha\,\bar{R}_0 = 0$$

Where

$$\overline{N} = \frac{\sin^2\theta}{\overline{\kappa}}(\sin\theta\overline{p'}_1 - \overline{p_2}\overline{\tau} + \overline{p_3}\overline{\kappa}) + \frac{\sin\theta\theta'}{\overline{\kappa}}(\sin\theta\overline{p'}_2 + \overline{p_1}\overline{\tau})$$

$$\overline{p}_1 = -1.3\sin\theta\overline{\kappa'}$$

$$\overline{p_2} = -0.3\overline{\kappa}\overline{\tau}$$

$$\overline{p_1'} = -1.3(\sin\theta\overline{\kappa''} + \overline{\kappa'}\cos\theta\theta')$$

$$\overline{p_2'} = -0.3(\overline{\kappa'}\overline{\tau} + \overline{\kappa}\overline{\tau'})$$

$$\alpha = arc\tan\frac{\overline{v_b}\cos\theta + \overline{v}}{\overline{v_b}\sin\theta + 2\pi\overline{R_0}(\overline{n_1} - \overline{n_0})}$$

$$\overline{\kappa} = \left|\overline{\ddot{\mathbf{R}}}\right| = \sin\theta\sqrt{\theta'^2 + \sin^2\theta}$$

$$\overline{\kappa'} = \frac{\theta'}{\sqrt{\theta'^2 + \sin^2\theta}}(\theta''\sin\theta + \theta'^2\cos\theta + 2\sin^2\theta\cos\theta)$$

$$\overline{\kappa''} = \frac{1}{\sqrt{\theta'^2 + \sin^2\theta}}\begin{pmatrix}\theta''^2\sin\theta + \theta'''\theta'\sin\theta + \theta''\theta'^2\cos\theta + 3\theta'^2\theta''\cos\theta \\ -\theta'^4\sin\theta + 2\theta''\sin^2\theta\cos\theta + 4\theta'^2\sin\theta\cos^2\theta - 2\theta'^2\sin^3\theta\end{pmatrix}$$
$$-\frac{\theta'(\theta''\sin\theta + \theta'^2\cos\theta + 2\sin^2\theta\cos\theta)}{(\theta'^2 + \sin^2\theta)^{\frac{3}{2}}}(\theta'\theta'' + \sin\theta\cos\theta\theta')$$

$$\overline{T} = \frac{1}{2\pi}\dot{\overline{\phi}}$$

$$\overline{\tau} = \dot{\overline{\phi}} + \sin\theta\cos\theta = 2\pi\overline{T} + \sin\theta\cos\theta$$

$$\overline{\tau'} = 2\pi\overline{T'} + \theta'(\cos^2\theta - \sin^2\theta)$$

The boundary conditions become

$$\overline{l_{AB}}\cos\theta_{AB} + \overline{l_{CD}}\cos\theta_{CD} = 0,\ \ \overline{n}_1 = (\overline{T_{AB}} - k)\eta,\ \ \overline{p_{3\mathrm{AB}}}\ \ \text{and}\ \ \overline{T_{\mathrm{CD}}}. \qquad (19)$$

3. Numerical computation

The finite difference method (Yin et al. 2016) for the numerical solution was applied to solve the equations presented in this paper. The transformed equations were integrated numerically over the domain $0 \le \psi \le \varphi$. The solutions were found by the following scheme: First, initialize the known parameters and input the four boundary values. Next, create trial matrix $\mathbf{X}_0$ which was composed of unknown variables $\overline{p_{3i}}$, θ_i, $\overline{T_i}$. Then, create a trial value for $\bar{n}_1$. After that, the Jacobian matrix was generated and iterated by the Newton-Raphson scheme until the norm of the functions was smaller than 10^{-5}. If the results of two adjacent iteration for $\bar{n}_1$ was larger than 10^{-5}, use the new $\bar{n}_1$ as trial values for iteration. Finally, the three unknown variables and one unknown constant value were obtained.

The parameter values used in numerical computation are shown as follows, $\overline{T_{CD}}=1$, $\overline{p_{3CD}}=600$, $\bar{R}_0=0.03$, $\bar{v}=1e3$, $\bar{v}_b=\bar{v}$, $\bar{n}_0=\bar{v}\overline{T_{CD}}$, μ=0.8, φ=60^o, $\overline{l_{AB}}=\overline{l_{CD}}$ unless otherwise stated.

3.1 Effects of wrap angle

Fig. 7 shows yarn performance at different wrap angles of 30^o, 60^o, and 90^o. Fig. 7 a-c display yarn spatial positions lying on a moving cylinder at three different wrap angles. For small wrap angles, the yarn spatial curve can be simplified as an in-plane curve due to the approximate constant value of the deviation angle close to 90^o. As the wrap angle increases, a more curved spatial yarn path can be obtained. Fig. 7d shows the effect of wrap angle on yarn tension distribution. Since the yarn tension was controlled at the exit point of the cylinder, a large wrap angle leads to a low yarn tension at the entrance point of the cylinder. Moreover, a linear relationship can be found between the yarn tension and the wrap angle. Fig. 7e reflects the effect of wrap angle on yarn twist distribution. The larger the wrap angle, the higher the twist difference between two ends of the yarn lying on a solid cylinder. As the wrap angle increases from 30^o to 90^o, yarn twist in zone AB increases from 1.86 to 3.12. The change of warp angle has proven to be the most effective way to affect the false twisting efficiency, propagation coefficients of twist trapping and congestion (Yin et al. 2020a). Fig. 7f demonstrates the bending and torsional moments under 3 different wrap angles. In the cases of wrap angle of 30^o, 60^o and 90^o, the mean values of bending and torsional moments are 1.51, 1.47, 1.41, and 9.14, 11.71, 14.08, respectively. Therefore, it is clear that in all cases the bending and torsional moments are of the same order of magnitude, and ignoring the bending moment may lead to errors in the simulation results.

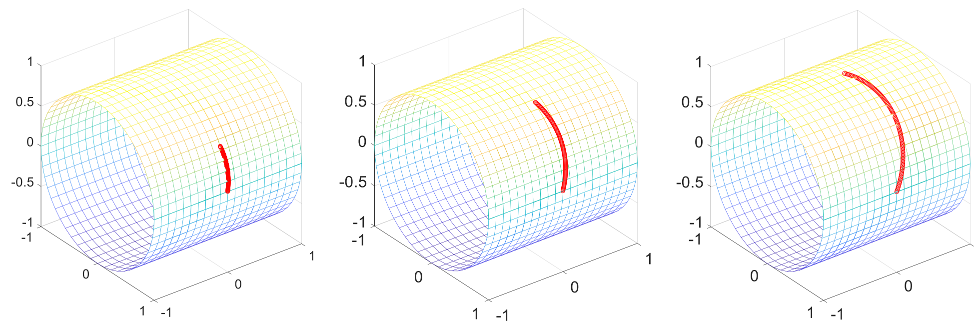

(a) $\varphi=\dfrac{\pi}{6}$ (b) $\varphi=\dfrac{\pi}{3}$ (c) $\varphi=\dfrac{\pi}{2}$

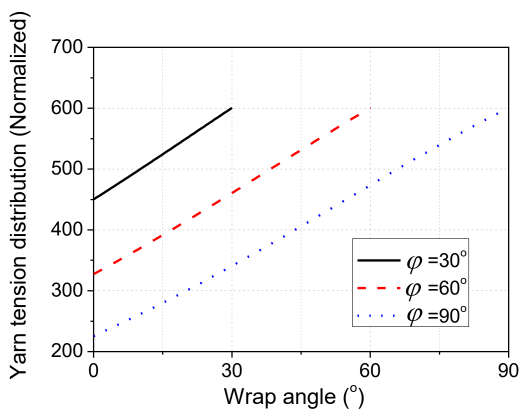

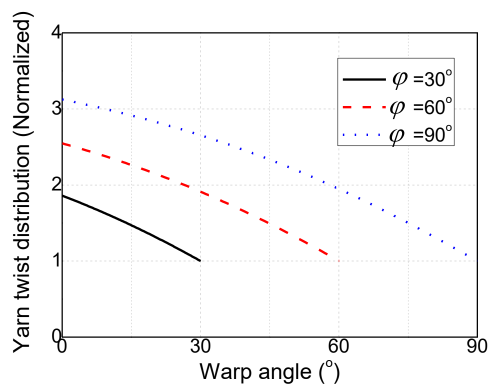

(d) The effect of φ on $\overline{p_3}$ (e) The effect of φ on $\overline{T}$

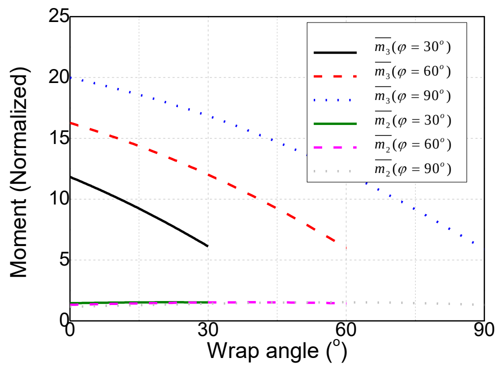

(f) The effect of φ on $\overline{m}$

Fig. 7 The effect of wrap angle on yarn performance

3.2 Effects of moving speed of the solid cylinder

Fig. 8 shows yarn performance at different moving speeds of the solid cylinder. Fig. 8a shows the effect of $\overline{v_b}$ on yarn tension distribution. As $\overline{v_b}$ increases from $0.5\bar{v}$ to $1.5\bar{v}$, the mean yarn tenacity increases from 427.11 to 492.96. Fig. 8b displays the effect of $\overline{v_b}$ on yarn twist distribution. The increment of $\overline{v_b}$ also leads to a build-up in yarn twist. Fig. 8c illustrates the effect of $\overline{v_b}$ on deviation angle. The deviation angle determines the level of out-of-plane yarn spatial curvature, and another way to express yarn geometry position. The higher the slope, the higher the level of yarn curvature. When $\overline{v_b}$ is increased, the slope of the deviation angle is slightly increased as well. The bending and torsional moments against 3 cases of $\overline{v_b}$ are shown in Fig. 8d. The mean values of torsional and bending moments are still of the same order of magnitude, though the values of torsional moments are much larger than those of bending moments.

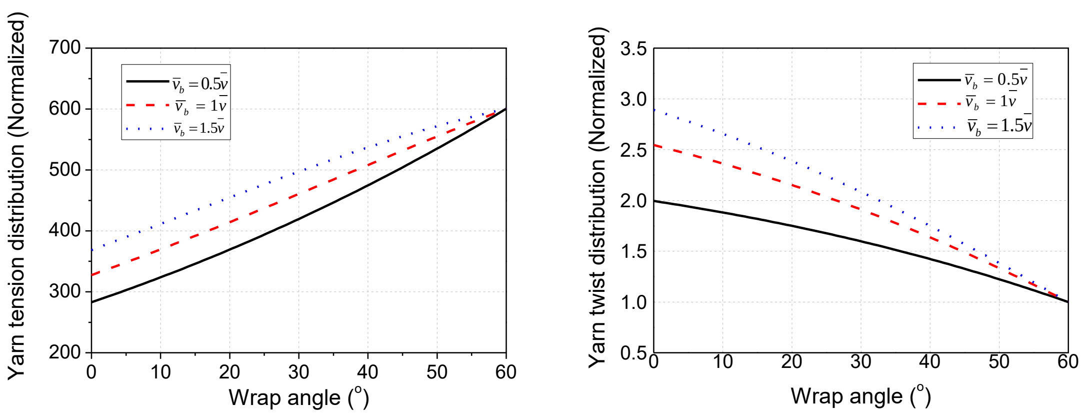

(a) The effect of $\overline{v_b}$ on $\overline{p_3}$ (b) The effect of $\overline{v_b}$ on $\overline{T}$

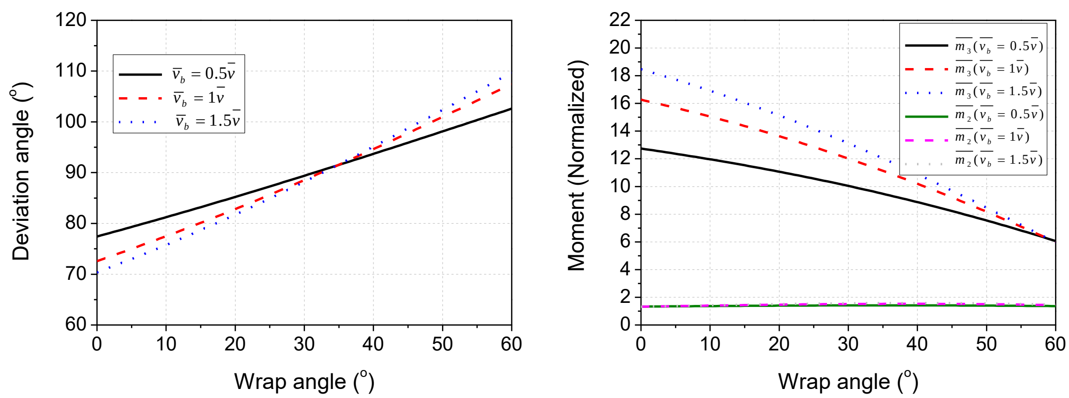

(c) The effect of $\overline{v_b}$ on θ (d) The effect of $\overline{v_b}$ on $\overline{m}$

Fig. 8 The effect of velocity of solid cylinder (normalized) on yarn performance

3.3 Effects of yarn radius

Fig. 9 shows yarn performance under different yarn radii $\overline{R_0}$. The effect of yarn radius has little influence on yarn tension distribution and yarn spatial position, as shown in Fig. 9a and c, but the effect on yarn twist distribution is greater, as shown in Fig. 9b. As the yarn radius increases from 0.015 to 0.045, the corresponding yarn twist at zone AB also increases from 1.63 to 3.96, which leads to a higher torsional moment as shown in Fig. 9d. In the case of $\overline{R_0}$ =0.045, the mean value of the torsional moment is an order of magnitude larger than the bending moment.

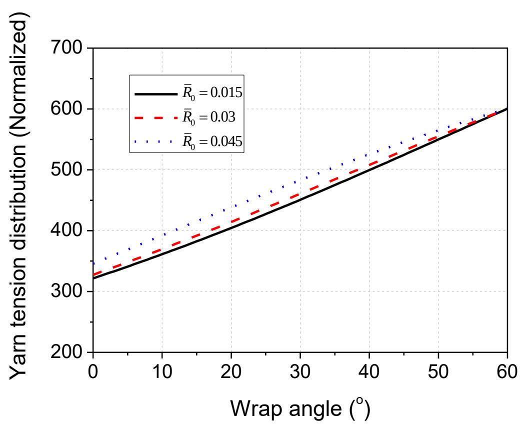

(a) The effect of $\overline{R_0}$ on $\overline{p_3}$

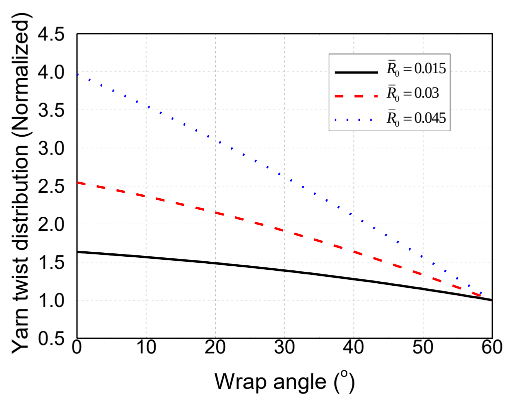

(b) The effect of $\overline{R_0}$ on $\overline{T}$

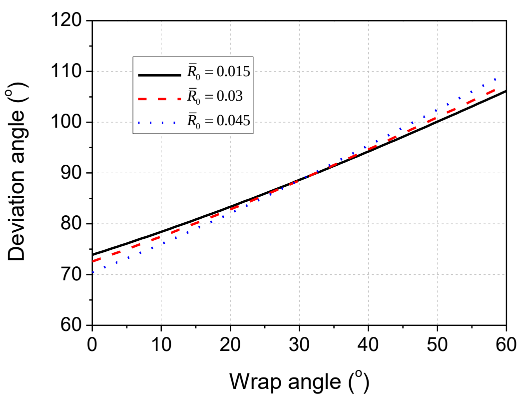

(c) The effect of $\overline{R_0}$ on θ

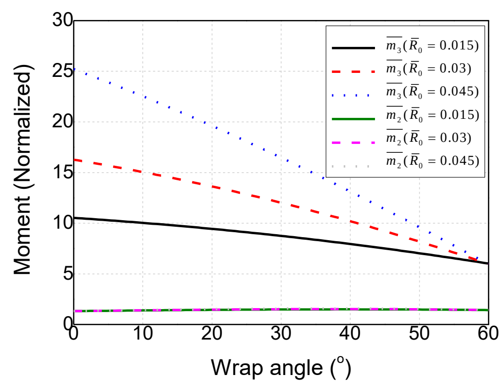

(d) The effect of $\overline{R_0}$ on $\overline{m}$

Fig. 9 The effect of yarn radius (normalized) on yarn performance

3.4 Effects of yarn tension

Fig. 10 shows yarn performance under different yarn tensions. The change of $\overline{p_{3\mathrm{CD}}}$ greatly influences yarn tension and twist distributions. As $\overline{p_{3\mathrm{CD}}}$ increases, both the mean yarn tension and twist are built-up, as shown in Fig. 10a and b. However, the effect of $\overline{p_{3\mathrm{CD}}}$ has no influence on yarn geometry position, as displayed in Fig. 10c. The effect of $\overline{p_{3\mathrm{CD}}}$ on yarn bending and torsional moments are shown in Fig. 10d, and a similar trend for yarn twist can also be found.

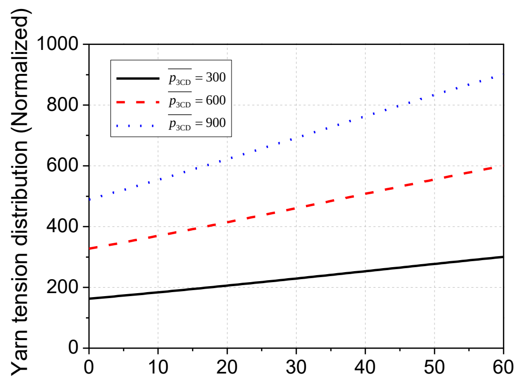

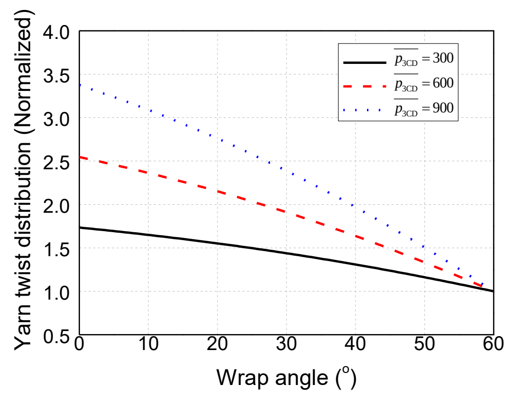

(a) The effect of $\overline{p_{3\mathrm{CD}}}$ on $\overline{p_3}$ (b) The effect of $\overline{p_{3\mathrm{CD}}}$ on $\overline{T}$

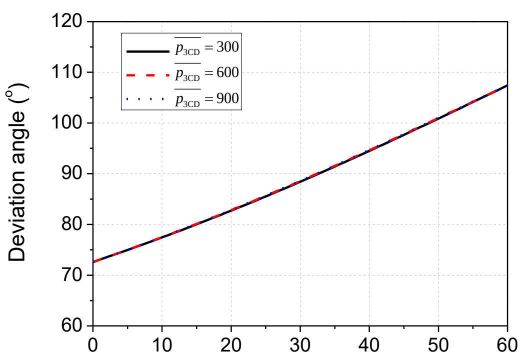

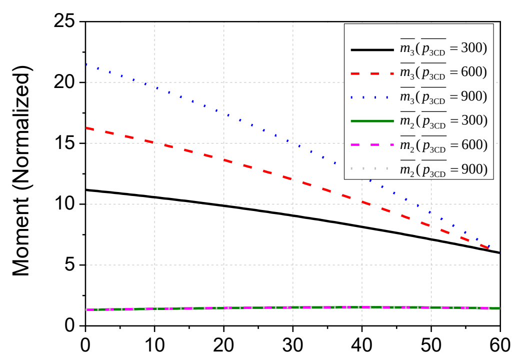

(c) The effect of $\overline{p_{3\mathrm{CD}}}$ on θ (d) The effect of $\overline{p_{3\mathrm{CD}}}$ on $\overline{m}$

Fig. 10 The effect of yarn tension (normalized) on yarn performance

3.5 Effects of yarn twist

Fig. 11 shows yarn performance under different yarn twists. The change of $\overline{T_{\mathrm{CD}}}$ has little influence on the yarn tension distribution and the yarn geometry position, as shown in Figs. 11a and c, but does have a large influence on the distribution of yarn twist as well as the yarn torsional moment, as shown in Fig. 11b and d.

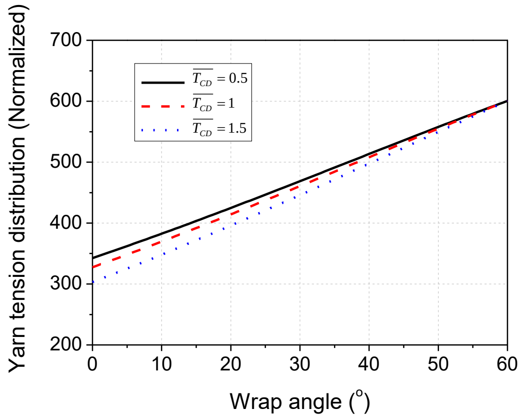

(a) The effect of $\overline{T_{\mathrm{CD}}}$ on $\overline{p_3}$

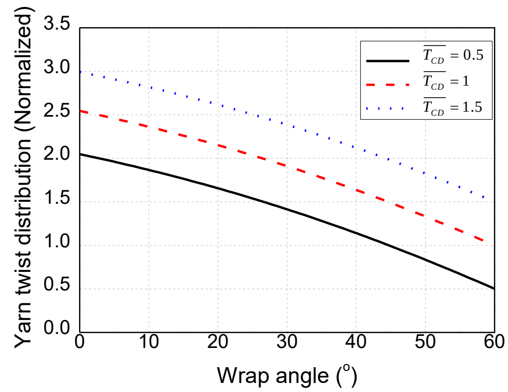

(b) The effect of $\overline{T_{\mathrm{CD}}}$ on $\overline{T}$

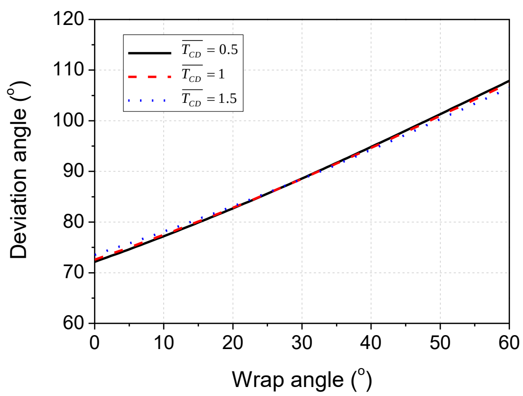

(c) The effect of $\overline{T_{\mathrm{CD}}}$ on θ

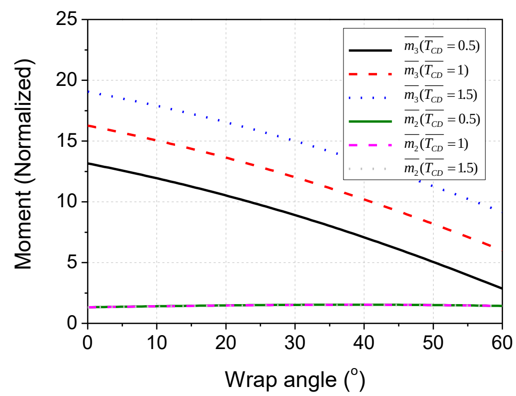

(d) The effect of $\overline{T_{\mathrm{CD}}}$ on $\overline{m}$

Fig. 11 The effect of yarn twist (normalized) on yarn performance

3.6 Effects of frictional coefficient

Fig. 12 shows yarn performance for various coefficients of friction between the yarn and the cylindrical solid. In Fig. 12a, the three curves of yarn tension distribution present an approximately linear relationship with the wrap angle. A higher coefficient of friction can lead to a larger reduction in yarn tension. In Fig. 12b, an increase in the coefficient of friction leads to an increase in the normalized twist distribution. As expected, a higher coefficient of friction gives rise to a more curved figure of the yarn path on the solid cylinder, as shown in Fig. 12c. The torsional moment of the yarn also increases as a result of increased yarn twist, as shown in Fig. 12d.

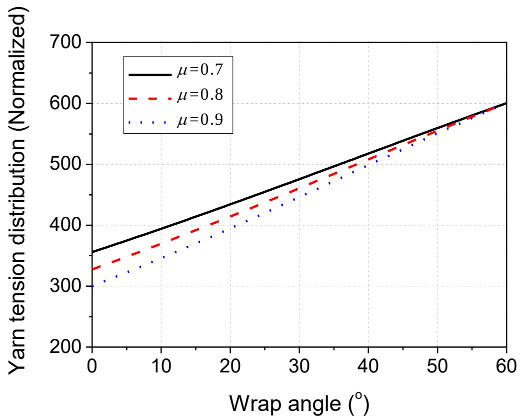

(a) The effect of μ on $\overline{p_3}$

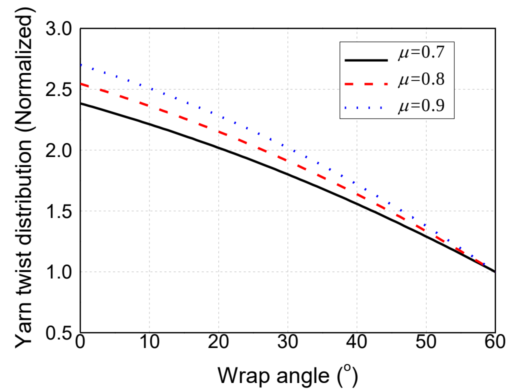

(b) The effect of μ on $\overline{T}$

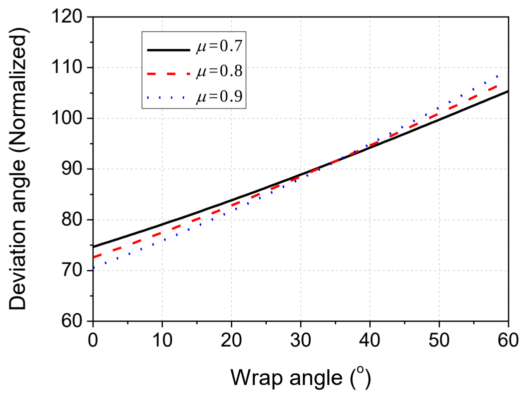

(c) The effect of μ on θ

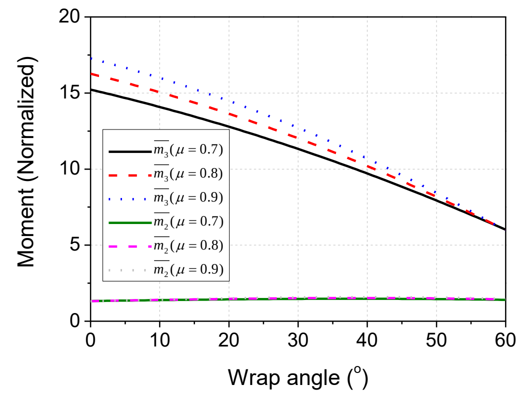

(d) The effect of μ on $\overline{m}$

Fig. 12 The effect of frictional coefficient on yarn performance

4. Experimental

Experiments were conducted on a ring spinning machine (Zinser 351) with a moving solid cylinder made of polyurethane with a diameter of 6 mm, sitting between the front rollers and yarn guide. Cotton yarn with a linear density of 18.45 g/km and diameter of 0.16 mm were spun for the experiments. The yarn tension was measured by a strain gauge sensor (Honigmann tension meter 125.12, 100cN maximum range, 0.1cN precision, 15° measuring angle), and the yarn twist was measured by a high-speed camera (Phantom MIRO 4, CMOS sensor, 800 × 600 pixels, over 1200 fps at full resolution, 22 µm pixel size, 12-bit depth). Before measurement, both the yarn tension meter and the high-speed camera system were calibrated. In addition, the coefficient of friction of the yarn and the rigid cylinder was 0.81, measured by a Shirley friction meter. The torsional rigidity of the yarns was measured by a KES yarn torsion and intersecting torque tester. Three sets of experiments were conducted as listed in Table 1

Based on the parameters given in Table 1, simulation results of the distribution of yarn twist, tension, and deviation angle lying on the solid cylinder for the three cases were obtained. Table 2 lists the simulated and measured values and errors of yarn tension, twist, and deviation angle at l_{AB}. In all three cases, the errors between the simulated values and experimental data were lower than 10%, which indicates that a good agreement has been made between the model prediction and experimental results. Additionally, it was noted that the variation in the twist and angle measurements were larger than 14%, which may be caused by the relative motion of the yarn on the moving solid cylinder.

Table 1 Parameters for case study

Case	φ (^{o})	T_{CD} (tpm) [CV%]	p_{3CD} (cN) [CV%]	K ($1e^{-9}Nm^2$) [CV%]	v (m/s)	$\frac{\overline{v}_b}{v}$
1	50	902 [14.55]	16.53 [5.32]	4.87 [14.43]	0.16	2
2	50	563 [18.23]	14.20 [7.54]	2.51 [13.23]	0.25	2
3	50	562 [15.44]	19.82 [6.23]	2.73 [12.34]	0.25	2

Table 2 Comparisons between the simulated values and experimental observations

Case	p_{3AB} (cN)			T_{AB} (tpm)			θ_B (^{o})		
	M [CV %]	S	E (%)	M [CV %]	S	E (%)	M [CV %]	S	E (%)
1	10.61	9.61	9.43	1217	1180	3.04	77.9	73.09	6.17

	[7.22]			[14.22]			[15.89]		
2	10.03 [5.48]	9.71	3.19	943 [14.57]	966	2.44	76.7 [20.67]	72.66	5.27
3	14.07 [5.89]	13.79	1.99	1157 [15.41]	1091	5.70	77.9 [14.51]	72.46	6.98

Note that M, S and E represent the measured value, simulated value, and error, respectively.

The simulation results of this study were compared with the results of an earlier model and with experiment (see Fig. 13). Compared with an earlier model in which bending was ignored, our simulation results of the current model show lower tension but higher twist values. As shown in Fig. 13a, the tension values predicted by our current model are closer to but slightly lower than measured experiment for all three cases, while the tension values simulated by a previous model predict slightly higher values than experimentally observed. In terms of yarn twist, the current model can also obtain a more accurate prediction than the previous model (which ignored bending) when compared with the experimental results, as shown in Fig. 13b.

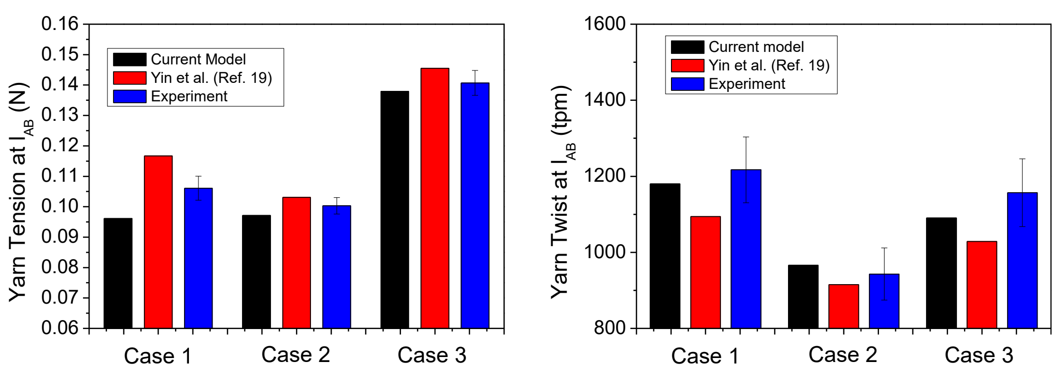

(a) Yarn tensions at l_{AB} for 3 cases (b) Yarn twists at l_{AB} for 3 cases

Fig. 13 Comparisons among the current and previous models and experiments

5. Conclusions

In this paper, the performance of a twisted yarn constrained to lie on a solid cylinder has been studied. Equations of motion were established based on Cosserat theory. The boundary value problems were numerically solved by the Newton-Raphson method. The effects of various spinning parameters in terms of wrap angle, speed of the moving cylinder, yarn diameter, yarn tension, yarn twist, and frictional coefficient, on yarn tension and twist distributions, yarn spatial position, bending and torsional moments lying on a cylinder were discussed. The results suggested that in most cases the bending and torsional moments are of the same order of magnitude, and so the effect of bending should not be neglected. Moreover, among all of the parameters investigated, wrap angle is the most significant factor affecting yarn twist and tension distributions as well as yarn spatial position lying on a cylinder. Experiments of the modified ring spinning system were conducted to verify the theoretical work and a good agreement has been made between model prediction and experiment. In addition, some simulation results and experimental data of this study were compared with results from an earlier model. It was found that the current model can give a more accurate prediction than a previous model by incorporating a bending term. The results gained from this study will enrich our understanding of the modified ring spinning process and provide a better handle of predicting how cellulose fibers can add better value down the supply chain.

Acknowledgment

This research was funded in part through a research grant from the Innovation and Technology Commission of the Hong Kong Special Administrative Region, China (Project No: ITP/021/17TI) and a postgraduate scholarship by the Hong Kong Polytechnic University.

Conflict of interest statement

The authors declare that they have no conflict of interest.

References

Bennett JM, Postle R (1979) A study of yarn torque and its dependence on the distribution of fiber tensile stress in the yarn part II: Experimental J Text I 70:133-141

César NR, Pereira-da-Silva MA, Botaro VR, de Menezes AJ (2015) Cellulose nanocrystals from natural fiber of the macrophyte Typha domingensis: extraction and characterization Cellulose 22:449-460

Feng J, Xu BG, Tao XM (2012) Dynamic measurement and modelling of flexible yarn dynamic behaviour on a moving cylindrical solid structure Meas Sci Technol 23

Fraser W (1993) On the theory of ring spinning P Roy Soc Lond A Mat 342:439-468

Fraser W, Stump D (1998) The equilibrium of the convergence point in two-strand yarn plying Int J Solids

Struct 35:285-298
Grosberg P, Oxenham W, Miao M (1987) The Insertion of ‘Twist’into Yarns by Means of Air-jets. Part II: Twist Distribution and Twist-insertion Rates in Air-jet Twisting J Text I 78:204-219
Guo BP, Tao XM, Lo TY (2000) A mechanical model of yarn twist blockage in rotor spinning Text Res J 70:11-17
Guo Y, Feng J, Yin R, Wang XG, van der Sluijs M, Tao XM (2015) Investigation and evaluation on fine Upland cotton blend yarns made by the modified ring spinning system Text Res J 85:1355-1366
Hearle JWS, Grosberg P, Backer S (1969) Structural Mechanics of Fibers, Yarns, and Fabrics. Wiley-Interscience, New York
Hua T, Tao XM, Cheng KPS, Xu BG, Huang XX (2013) An experimental study of improving fabric appearance of denim by using low torque singles ring spun yarns Text Res J 83:1371-1385
Kim T-K, Son Y-A (2005) Effect of reactive anionic agent on dyeing of cellulosic fibers with a Berberine colorant—part 2: anionic agent treatment and antimicrobial activity of a Berberine dyeing Dyes Pigments 64:85-89
Lawrence CA (2010) Advances in yarn spinning technology. Woodhead Publishing Ltd, Cambridge
Liu X-h, Zhang Q-y, Cheng B-w, Ren Y-l, Zhang Y-g, Ding C (2018) Durable flame retardant cellulosic fibers modified with novel, facile and efficient phytic acid-based finishing agent Cellulose 25:799-811
Liu Y, Xie J, Wu N, Ma Y, Menon C, Tong J (2019) Characterization of natural cellulose fiber from corn stalk waste subjected to different surface treatments Cellulose 26:4707-4719
Love AEH (1927) A Treatise on The Mathematical Theory of Elasticity. Cambridge University Press, Cambridge
Miao M, Chen R (1993) Yarn twisting dynamics Text Res J 63:150-158
Morán JI, Alvarez VA, Cyras VP, Vázquez A (2008) Extraction of cellulose and preparation of nanocellulose from sisal fibers Cellulose 15:149-159
Stump DM, Fraser WB (1996) Transient solutions of the ring-spinning balloon equations J Appl Mech-T Asme 63:523-528
Tandon S, Kim S, Choi F (1995) The torsional behaviour of singles yarns. Part II: Evaluation J Text I 86:200-217
Tang H, Xu B, Tao X, Feng J (2011) Mathematical modeling and numerical simulation of yarn behavior in a modified ring spinning system Appl Math Model 35:139-151
Tao XM, Yin R (2019) Apparatus and Method for Imparting False Twist to a Yarn.
van der Heijden GHM, Champneys AR, Thompson JMT (2002) Spatially complex localisation in twisted elastic rods constrained to a cylinder Int J Solids Struct 39:1863-1883
van der Heijden GHM, Thompson JMT (2000) Helical and localised buckling in twisted rods: A unified analysis of the symmetric case Nonlinear Dynam 21:71-99
Xu BG, Tao XM (2003) Integrated approach to dynamic analysis of yarn twist distribution in rotor spinning Text Res J 73:79-89
Yang K, Tao XM, Xu BG, Lam J (2007) Structure and properties of low twist short-staple singles ring spun yarns Text Res J 77:675-685
Yin R, Gu H-b (2011a) Numerical simulation of quasi-stationary ring spinning process linear elastic yarn Text Res J 81:22-27
Yin R, Gu H (2011b) Accurate prediction of the ring‐spinning equation in zero air drag based on homotopy perturbation method J Text I 102:763-766
Yin R, Liu Y, Gu H Artificial parameter perturbation method and parameter-expansion method used in accurate prediction of the ring-spinning balloon in zero air drag. In: 2010 International Conference on System Science, Engineering Design and Manufacturing Informatization, 2010. IEEE, pp 222-225
Yin R, Tao X-M, Xu B-g (2020a) Systematic investigation of twist generation and propagation in a modified ring spinning system Text Res J 90:367-375
Yin R, Tao X-M, Xu B-g (2020b) Yarn and fabric properties in a modified ring spinning system considering the effect of the friction surface of the false-twister Text Res J 90:572-580
Yin R, Tao X, Xu B (2016) Mathematical modeling of yarn dynamics in a generalized twisting system Sci Rep-Uk 6:24432
Yin R, Tao X, Xu B (2018) Variation of false twist on spinning process stability and resultant yarn properties in a modified ring spinning frame Text Res J 88:1876-1892